European Journal of Medicinal Chemistry 50 (2012) 319–331

Contents lists available at SciVerse ScienceDirect

European Journal of Medicinal Chemistry

journal homepage: http://www.elsevier.com/locate/ejmech

Original article

Photoactivated DNA cleavage and anticancer activity of pyrenyl-terpyridine lanthanide complexes

Akhtar Hussain [a], Sudarshan Gadadhar [b], Tridib K. Goswami [a], Anjali A. Karande [b,**], Akhil R. Chakravarty [a,*]

[a] Department of Inorganic and Physical Chemistry, Indian Institute of Science, Sir C.V. Raman Avenue, Bangalore 560012, India
[b] Department of Biochemistry, Indian Institute of Science, Sir C.V. Raman Avenue, Bangalore 560012, India

ARTICLE INFO

Article history:
Received 16 November 2011
Received in revised form
1 February 2012
Accepted 3 February 2012
Available online 10 February 2012

Keywords:
Medicinal chemistry
Lanthanide complexes
Pyrenyl-terpyridine photosensitizer
Crystal structure
Photocytotoxicity
Cellular imaging

ABSTRACT

Lanthanide(III) complexes [Ln(R-tpy)(acac)$(NO_3)_2$] (Ln = La(III) in **1**, **2**; Gd(III) in **4**, **5**) and [Ln(py−tpy)(sacac)$(NO_3)_2$] (Ln = La(III), **3**; Gd(III), **6**), where R-tpy is 4′-phenyl-2,2′:6′,2″-terpyridine (ph−tpy in **1**, **4**), 4′-(1-pyrenyl)-2,2′:6′,2″-terpyridine (py−tpy in **2**, **3**, **5** and **6**), acac is acetylacetonate and sacac is 4-hydroxy-6-{4-[(β-D-glucopyranoside)oxy]phenyl}hex-3,5-dien-2-onate, were prepared to study their DNA photocleavage activity and photocytotoxicity. Complexes [La(ph-tpy)(acac)(EtOH)$(NO_3)_2$] (**1a**) and [Gd(ph−tpy)(acac)$(NO_3)_2$] (**4**) were characterized by X-ray crystallography. The 1:1 electrolytic complexes bind to calf thymus DNA. The py−tpy complexes cleave pUC19 DNA and exhibit remarkable photocytotoxicity in HeLa cells in UV-A light of 365 nm with apoptotic cell death (IC_{50}: ~40 nM in light, >200 μM in dark). Confocal microscopy using HeLa cells reveal primarily cytosolic localization of the complexes.

1. Introduction

Metal-based photoactivated chemotherapeutic agents are of current interests for their potential utility in the photodynamic therapy (PDT) of cancer [1–4]. PDT has emerged as a new modality of cancer cure due to its non-invasive nature and for its selectivity in which the photo-irradiated cancer cells are selectively damaged leaving the unexposed normal cells intact [5–8]. The currently used PDT agents are primarily porphyrin and phthalocyanine bases. The mode of action of the organic PDT agents is to generate cytotoxic singlet oxygen ($^1O_2$) upon photoactivation involving the $^3(\pi\text{-}\pi^*)$ state of the photosensitizer and molecular oxygen ($^3O_2$) [9–11]. The major drawbacks of such bases include skin sensitivity and hepatotoxicity which leads to jaundice [12,13]. Besides, the potency of an organic PDT agent depends largely on the high quantum yield of singlet oxygen generation which is often difficult to achieve thus making them unsuitable for phototherapeutic applications [11]. These problems could be circumvented using metal-based PDT agents which could be suitably designed utilizing tunable coordination geometries, wide spectral and redox properties thus providing alternate type-I and/or photo-redox pathways to cause cellular photodamage in addition to the generation of singlet oxygen species in a type-II process. The 4*d* and 5*d* metal-based anticancer agents, *viz.*, platinum(IV), ruthenium(II) and rhodium(II) complexes, are reported to display photocytotoxicity in a variety of cancer cells [14–19].

Our work on the 3*d* metal-based complexes has shown that iron(III) and oxovanadium(IV) complexes are remarkably photocytotoxic in various cancer cells in visible light [20–24]. While transition metal-based PDT agents are reported from various research groups, the lanthanide-based PDT agents are virtually

Abbreviations: AO, acridine orange; CCDC, Cambridge Crystallographic Data Centre; ct-DNA, calf thymus DNA; DABCO, 1,4-diazabicyclo[2.2.2]octan; DMEM, Dulbecco's Modified Eagle's Medium; DMF, dimethylformamide; DMSO, dimethyl sulfoxide; DNA, deoxyribonucleic acid; DOTA, 1,4,7,10-tetraazacyclododecane-1,4,7,10-tetraacetate; dppz, dipyrido[3,2-a:2′,3′-c]phenazine; DTPA, diethylenetriaminepentaacetate; EB, ethidium bromide; EDTA, ethylenediaminetetraacetate; FBS, foetal bovine serum; GLUTs, glucose transporters; ISC, intersystem crossing; MTT, 3-(4,5-dimethylthiazol-2-yl)-2,5-diphenyltetrazolium bromide; MvH, McGhee-von Hippel; NC, nicked circular; PBS, phosphate buffered saline; PDT, photodynamic therapy; PI, propidium iodide; RME, receptor-mediated endocytosis; SC, supercoiled; SOD, superoxide dismutase; TEMP, 2,2,6,6-tetramethyl-4-piperidone.

* Corresponding author. Tel.: +91 80 22932533.
** Corresponding author. Tel.: +91 80 22932306.
E-mail addresses: anjali@biochem.iisc.ernet.in (A.A. Karande), arc@ipc.iisc.ernet.in (A.R. Chakravarty).

0223-5234/$ – see front matter © 2012 Elsevier Masson SAS. All rights reserved.
doi:10.1016/j.ejmech.2012.02.011

unknown except few complexes containing macrocyclic organic dyes [25–27]. For example, a lutetium(III) texaphyrin (LUTRIN®) complex is an effective PDT agent in near-IR light of 732 nm [25]. The lanthanide complexes are being used as luminescent tags for bio-analytical applications [28–30]. Gadolinium(III) complexes, *viz*., $[Gd(DTPA)(H_2O)]^{2-}$ (Magnevist™) and $[Gd(DOTA)(H_2O)]^{-}$ (Dotarem™), are used as magnetic resonance imaging (MRI) contrast agents [31–33]. The success of the Gd-based MRI agents provides strong impetus to design new lanthanide complexes and explore their photochemotherapeutic potentials. The present work stems from our continued interest to enrich the chemistry of photocytotoxic Ln(III) complexes using their high coordination number and oxophilicity [34,35].

We have chosen terpyridine bases as photoactive organic ligands to achieve high photocytotoxicity in cancer cells. The Ln(III) complexes are expected to be non-toxic in dark owing to their redox stability thus making them suitable for cellular applications in the presence of reducing thiols, *viz*., glutathione. We have recently reported the La(III) and Gd(III) complexes $[Ln(dppz)_2(NO_3)_3]$ and $[Ln(dppz)(acac)_3]$ of dipyridophenazine (dppz) as DNA photocleaving agents showing photocytotoxicity in HeLa cells on irradiation with UV-A light of 365 nm while remaining essentially non-toxic in dark [34,35]. We have now designed and synthesized a series of lanthanide complexes having pyrene-appended terpyridine and acetylacetonate as ligands. The choice of pyrenyl terpyridine (py–tpy) as a ligand is based on the fact that tpy with a pendant pyrenyl moiety could serve as a photosensitizer-cum-DNA binder. The photoactive pyrenyl moiety, also being a fluorophore, could be used for confocal fluorescence microscopy to study the localization of the complex within the cancer cell and for its cytotoxicity on photoactivation. We have also prepared the corresponding phenyl analogues (ph–tpy complexes) as controls to understand the role of the pyrenyl moiety in the cellular damage. The *O*,*O*-donor β-diketonate ligand is chosen for strong complexing nature of the oxophilic lanthanide ions resulting in the formation of a stable complex. We have also used a carbohydrate-appended acetylacetonate ligand to increase the aqueous solubility of the complexes and to augment their cancer cell targeting potential. There is an upregulation of glycolysis and a decrease in the oxidative phosphorylation in cancer cells compared to the normal cells which results in inefficiency in the metabolism of cancer cells. Consequently, the glucose requirements of cancer cells are significantly higher than the normal cells for their uncontrolled growth and proliferation resulting in the overexpression of certain proteins known as GLUTs which form a class of transmembrane proteins mediating the transport of glucose to the cells [36,37]. We have designed the present complexes based on our dual strategy of combining imaging with therapy. In addition, the presence of the nitrate anions in the complexes would improve their aqueous solubility. The use of tridentate terpyridine, as compared to the bidentate phenanthroline bases, has led to higher coordination number of the complexes thus decreasing the possibilty of any hydrolytic DNA damage since lanthanides are known to display significant hydrolytic DNA cleavage activity [38].

Herein, we report the synthesis, characterization, DNA binding, DNA cleavage activity and photocytotoxicity of the lanthanide(III) complexes $[Ln(R\text{-}tpy)(acac)(NO_3)_2]$ (Ln = La(III), **1** and **2**; Gd(III), **4** and **5**) and $[Ln(py–tpy)(sacac)(NO_3)_2]$ (Ln = La(III), **3**; Gd(III), **6**), where R-tpy is an *N*,*N*,*N*-donor ligand, *viz*., 4′-phenyl-2,2′:6′,2″-terpyridine (ph–tpy in **1**, **4**), 4′-(1-pyrenyl)-2,2′:6′,2″-terpyridine (py–tpy in **2**, **3**, **5** and **6**), acac is acetylacetonate and sacac is 4-hydroxy-6-{4-[(β-D-glucopyranoside)oxy]phenyl}hex-3,5-dien-2-onate (Scheme 1). Complexes **1** as $[La(py–tpy)(sacac)(EtOH)(NO_3)_2]$ (**1a**) and **4** were structurally characterized by single crystal X-ray diffraction method.

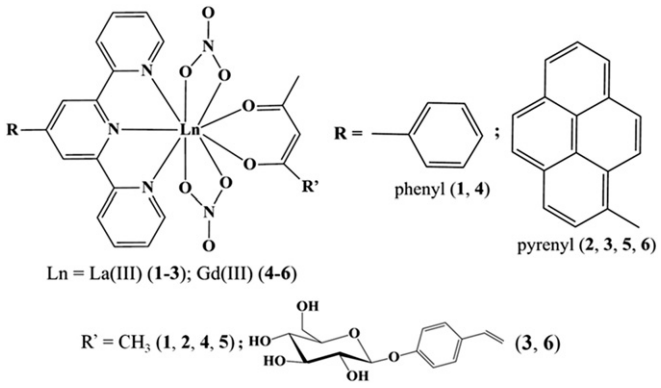

Scheme 1. Schematic drawing of the La(III) and Gd(III) complexes **1**–**6** and the ligands used.

Significant results of this study include remarkable photocytotoxicity (PDT effect) of the pyrenyl terpyridine complexes in HeLa cells in UV-A light, while being less toxic in the dark. The py–tpy complexes showed cytosolic localization as evidenced from the confocal fluorescence imaging studies.

2. Chemistry

The substituted terpyridine ligand (ph–tpy and py–tpy) was prepared by a reaction of the corresponding aldehyde with 2-acetylpyridine in the presence of NaOH and subsequent condensation of the intermediate product with ammonium acetate in refluxing ethanol [39,40]. The glucose appended β-diketone ligand (Hsacac) was prepared in five synthetic steps. D-Glucose was acylated to get β-D-glucose pentaacetate which was subsequently reacted with Br_2/red P to afford the highly reactive α-acetobromoglucose. The α-acetobromoglucose was reacted with para-hydroxy benzaldehyde in the presence of NaOH using tetrabutylammonium bromide as the phase transfer catalyst to obtain the corresponding β-glycoside which was subsequently reacted with 2,4-pentatedione in presence of boric anhydride using dry DMF as a solvent to get the acetyl protected β-diketone ligand [41]. Finally, the deprotection of the acetyl group by standard method afforded the desired glucose appended β-diketone ligand (Hsacac) in moderate yield. Lanthanide(III) complexes **1**–**6** were prepared by a general method in two synthetic steps. Reaction of a CH_2Cl_2 solution of ph–tpy or py–tpy with an ethanol solution of the corresponding metal nitrate afforded the precursor complex $[Ln(ph–tpy)(NO_3)_3]$ or $[Ln(py–tpy)(NO_3)_3]$ in good yield. The precursor complex upon reaction with Hacac or Hsacac in the presence of triethylamine gave the desired complex in high yield (Scheme 1).

3. Pharmacology

The lanthanide(III) complexes **1**–**6** were evaluated for their DNA binding, DNA cleavage, and cytotoxic activities. Binding studies for the complexes with ct-DNA were done using spectroscopic methods such as electronic absorption titration and DNA melting and hydrodynamic method, *viz*., solution viscosity measurement of complex bound ct-DNA. The DNA cleavage activity of the complexes was studied by determining the ability of each complex to convert the supercoiled (SC) form of DNA to its nicked circular (NC) form. Photocytotoxicity of the complexes was assessed against HeLa cells by MTT assay [42]. The mechanistic aspects of cell death was studied by EB/AO dual staining method using fluorescence microscopy of the HeLa cells in the presence or absence of the

complexes in UV-A light and in dark. The cellular localization studies were carried out on HeLa cells by confocal fluoresence microscopy using the blue light emitting fluorescent pyrenyl complexes of La(III).

4. Results and discussion

4.1. Synthesis and general aspects

Reaction of a dichloromethane solution of the ph–tpy or py–tpy ligand with an ethanol solution of the corresponding metal nitrate afforded the precursor complex [Ln(ph–tpy)$(NO_3)_3$] or [Ln(py–tpy)$(NO_3)_3$]. The desired complexes **1**–**6** were prepared by reacting the corresponding precursor complex with 3 equivalents of Hacac or Hsacac in the presence of three equivalents of triethylamine as a base (Scheme 1). The complexes were characterized from the analytical and mass spectral data. Selected physicochemical data are given in Table 1. The molar conductivity value of $\sim 10^5$ S cm^2 M^{-1} suggests 1:1 electrolytic nature of the complexes in aqueous DMF (1:5 v/v). The nitrate ligand is likely to dissociate from the complex in a solution phase to form 1:1 electrolyte. This is further supported from the ESI-MS spectral data in aqueous methanol or aqueous acetonitrile showing the presence of a prominent $[M\text{-}(NO_3)]^+$ peak corresponding to the loss of one nitrate anion. The complexes are thus formulated as [Ln(R-tpy)(acac/sacac)$(NO_3)_2$] in the solid state and as [Ln(R-tpy)(acac/sacac)(NO_3)](NO_3) in an aqueous phase (R = ph or py). The IR spectra of the complexes in the solid state showed three strong bands around 1585, 1515 and 1380 cm^{-1} corresponding to the C=O, C=C (β-diketonate) and NO_3^- stretching vibrations, respectively, indicating bidentate coordination of the β-diketonate and NO_3^- ligands [43]. The ^{1}H-NMR spectra of the diamagnetic La(III) complexes (**1**–**3**) showed characteristic spectral features of the metal-bound polypyridyl ligand and β-diketonates. The large J value of 15 Hz for the protons at the 5,6-positions of the coordinated β-diketonate sacac ligand indicates the presence of a conjugated C=C double bond [44]. Room temperature solution magnetic susceptibility measurements of the paramagnetic Gd(III) complexes (**4**–**6**) in DMSO-d_6 gave magnetic moment value of $\sim$8.0 μ_B suggesting the presence of seven unpaired electrons. The electronic absorption spectra of the complexes in DMF displayed an intense ligand centred $\pi \rightarrow \pi^*$ transition at $\sim$278 nm (Fig. 1). The py–tpy complexes showed an additional band centred at 350 nm assignable to the low lying intraligand $\pi \rightarrow \pi^*$ transitions [40]. The broad band centred at 350 nm, observed due to sacac ligand in complexes **3** and **6**, obscures the absorption features arising from the py–tpy ligand [41]. The ph–tpy complexes **1** and **4** in aqueous DMSO (1:4 v/v) displayed fluorescence spectral band around 350 nm when excited at 285 nm with respective quantum yield value of 0.04 and 0.02. The py–tpy complexes in aqueous DMSO (1:4 v/v) exhibited intense emission band at $\sim$420 nm when excited at 350 nm with fluorescence quantum yields in the range of 0.14–0.22 (Fig. 1). The ph–tpy and py–tpy ligands showed similar emission spectral properties (Table 1) [45]. The emission property of the py–tpy complexes allowed us to study the cellular internalization of these complexes by confocal fluorescence microscopy. The py-tpy complexes were tested for their susceptibility towards photbleaching under UV-A light illumination by monitoring the decrease (if any) in the emission intensity in the presence of dissolved oxygen [46]. The emission intensities were recorded at an interval of 5 min (upto 60 min) after irradiation of a 10 μM solution of the complex in aqueous DMSO (1:4 v/v) with UV-A light of 365 nm (100 W lamp). No significant decrease in the fluorescence intensity of the solution was observed during the time-course studied. This observation suggests the fact that the py–tpy complexes do not suffer any photobleaching under intense UV-A light illumination.

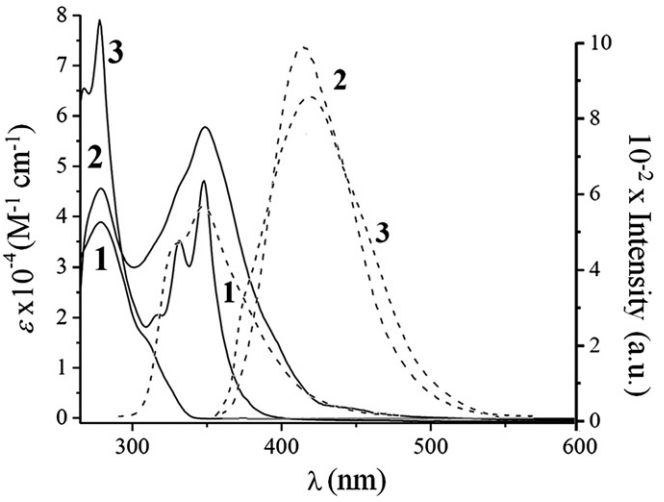

Fig. 1. Absorption spectra of **1**–**3** in DMF (solid curves). Fluorescence emission spectra (dotted curves) of **1**–**3** in 25% aqueous DMSO (excitation wavelengths are: 285 nm for **1** and 350 nm for **2** and **3**).

4.2. Crystal structure

Complexes **1** as [La(ph–tpy)(acac)(EtOH)$(NO_3)_2$] (**1a**) and **4** were structurally characterized by single crystal X-ray diffraction method. Both the crystals belonged to the triclinic space group $P\bar{1}$. The ORTEP views of the complexes are shown in Fig. 2. The complexes are discrete mononuclear species with the La(III) centre in a ten-coordinate LaO_7N_3 and Gd(III) centre in a nine coordinate GdO_6N_3 coordination geometry. The terpyridine ligand displays a tridentate mode of binding. The monoanionic acetylacetonate and two nitrate ligands bind in a bidentate chelating fashion. The coordination of a solvent ethanol molecule is observed in **1a**. The pyridine rings of the terpyridine moiety of ph–tpy ligand in complex **1a** are out of plane possibly due to coordination of the solvent ethanol molecule resulting in a *cis* disposition of two bidentate nitrate anions in the coordination sphere. In contrast, the pyridine rings of the ph–tpy ligand in complex **4** lie in a plane and a *trans*-disposition of two bidentate nitrate anions is observed. The OH group of the coordinated ethanol molecule in **1a** is hydrogen-bonded to the non-bound oxygen atom of one of the nitrate anions of another complex. In addition, the phenyl ring of the

Table 1
Selected physicochemical data and DNA binding parameters for the Ln(III) complexes **1**–**6**.

Complex	IR (cm^{-1})		μ_{eff} [a]	λ_f (nm) [Φ_f [b]]	M[c]	K_b (M^{-1}) [s][d]	ΔT_m [e] (°C)
	C=O	NO_3^-					
1	1595	1378		350 [0.04]	101	(4.6 ± 0.5) x 10^4 [0.2]	1.5
2	1580	1389		420 [0.22]	98	(2.9 ± 0.3) x 10^6 [0.5]	4.5
3	1581	1389		420 [0.18]	110	(9.8 ± 0.4) x 10^5 [0.4]	4.4
4	1590	1380	8.01	350 [0.02]	105	(5.0 ± 0.3) x 10^4 [0.3]	1.7
5	1581	1389	7.98	420 [0.15]	103	(3.2 ± 0.2) x 10^6 [0.6]	4.8
6	1584	1390	8.05	420 [0.12]	108	(9.5 ± 0.5) x 10^5 [0.5]	4.6

[a] μ_{eff} in μ_B using DMSO-d_6 solutions of the Gd(III) complexes at 25 °C.
[b] Emission spectral band in H_2O-DMSO (1:4 v/v). The quantum yield values of the ph–tpy and py–tpy ligands in H_2O-DMSO (1:4 v/v) are 0.06 and 0.34, respectively.
[c] Λ_M, molar conductivity in S cm^2 M^{-1} in 20% aqueous DMF at 25 °C.
[d] K_b, the calf thymus DNA binding constant [s, binding site size].
[e] Change in the calf thymus DNA melting temperature.

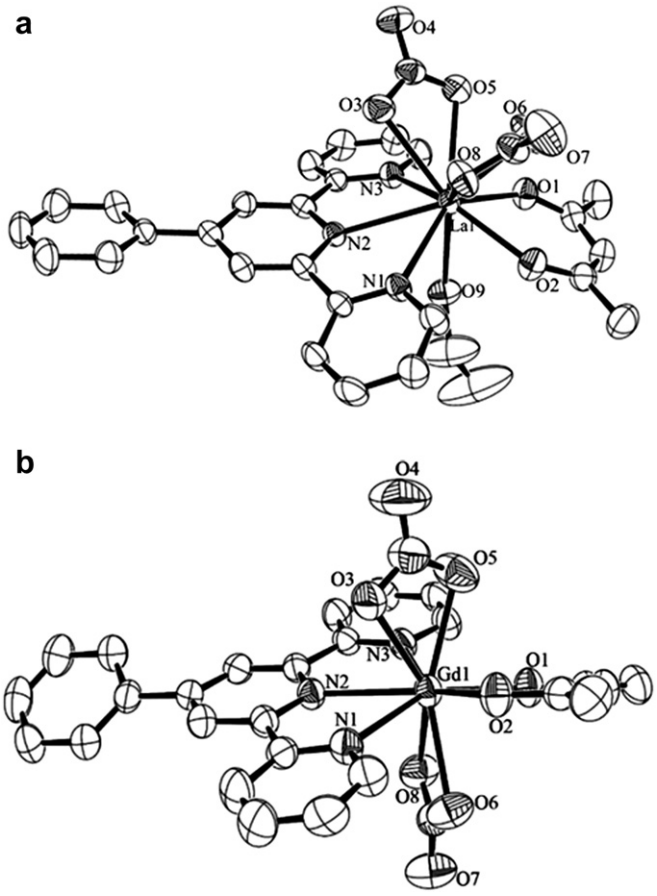

Fig. 2. ORTEP views of the complexes **1a** (a) and **4** (b) showing 50% probability thermal ellipsoids and the atom numbering scheme for the metal and hetero atoms. The hydrogen atoms are not shown for clarity.

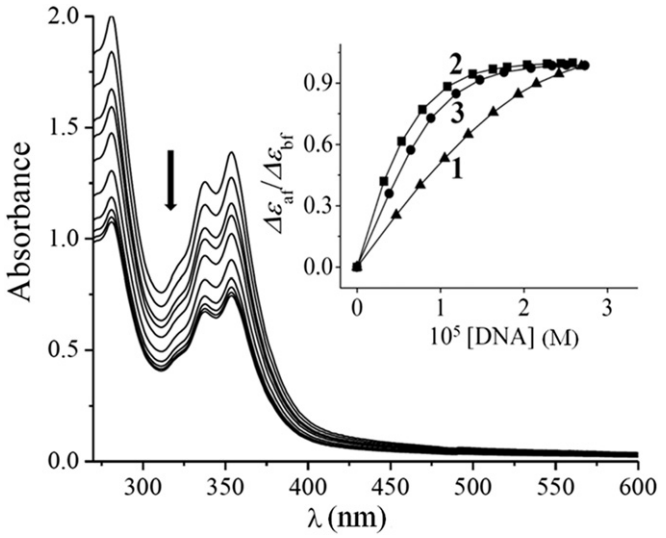

Fig. 3. Absorption spectral traces of complex **3** in 5 mM Tris–HCl buffer (pH 7.2) on increasing the quantity of calf thymus DNA. The inset shows the least-squares fit of $\Delta\varepsilon_{af}/\Delta\varepsilon_{bf}$ vs. [DNA] for [La(ph–tpy)(acac)$(NO_3)_2$] (**1**, ▲), [La(py–tpy)(acac)$(NO_3)_2$] (**2**, ●) and [La(py–tpy)(sacac)$(NO_3)_2$] (**3**, ■).

ph–tpy ligand makes an angle with the middle pyridine ring of the terpyridine moiety due to steric encumbrance among the aromatic hydrogen atoms giving a dihedral angle of 8.41° in complex **1a** and 26.39° in complex **2**. The La–O and La–N distances in complex **1a** are in the range of 2.398(2) to 2.722(3) Å and 2.711(3) to 2.731(3) Å, respectively. The Gd–O and Gd–N distances in complex **2** are in the range of 2.295(2) to 2.529(2) Å and 2.533(2)–2.576(2) Å, respectively. The Ln–O bond distances involving the acac ligand are shorter than those involving the nitrate ligands. The significantly long La(1)–O(6) and La(1)–O(8) bond lengths in **1a** that are trans to the ph–tpy ligand could result in the dissociation of the nitrate ligand in a polar solvent. The coordination behaviour observed in the present lanthanide complexes is similar to the previously reported structures for analogous lanthanide complexes [47].

4.3. DNA binding properties

4.3.1. Electronic absorption spectroscopy

DNA being one of the most important targets of many anticancer agents, designing and developing metal complexes that avidly bind to DNA are of paramount importance. The electronic absorption titrations were carried out to monitor the binding interactions of the complexes **1**–**6** with ct-DNA (Fig. 3). The intrinsic equilibrium ct-DNA binding constants (K_b) which give a measure of the strength of binding of a complex to ct-DNA are given in Table 1. The K_b values in the range of 10^4–10^6 M^{-1} follow the order: **6**, **5**, **3**, **2** > **1**, **4**. The py–tpy complexes have significantly higher K_b values than their ph–tpy analogues beacuse of the presence of a planar pendant pyrenyl moiety in the py–tpy ligand. This is expected since metal complexes of py–tpy are known to form π-assembled metallosupramolecular arrays supporting the fact that they can strongly π-stack in between the DNA base pairs [48]. The fitted parameter *s* of the MvH equation gives an estimate of the number of DNA bases associated with the complex and its value of <1.0 is typically interpreted as arising from the aggregation of hydrophobic molecules on the surface of DNA. The greater value of *s* for the py–tpy complexes than the ph–tpy analogues also indicates better DNA binding strength of the py–tpy complexes [49].

4.3.2. DNA melting studies

Thermal DNA denaturation experiments were performed to obtain insights into the binding of the complexes **1**–**6** to ct-DNA (Fig. 4(a)). A positive shift in the DNA melting temperature (ΔT_m) was observed upon addition of the complexes to the ct-DNA. The increase in the ct-DNA melting temperature suggests an increase in the stability of the double helix upon addition of the complex. The ΔT_m value of ~2 °C indicate primarily groove binding nature of the ph–tpy complexes to ct-DNA and a partial intercalative mode of binding of the py–tpy complexes to ct-DNA giving a large positive ΔT_m value of ~5 °C [50].

4.3.3. Viscosity measurements

Viscosity measurements were carried out to examine the effect of the complexes on the relative specific viscosity of the solution containing ct-DNA (Fig. 4(b)). Since the relative specific viscosity (η/η_0) of a solution containing DNA gives a measure of the increase in contour length of DNA associated with the separation of base pairs caused by intercalation, a classical intercalator, *viz*., ethidium bromide would result in a significant increase in the viscosity of the DNA solution (where η and η_0 are the respective specific viscosities of a DNA solution in the presence and absence of the complexes). In contrast, a partial and/or non-intercalating molecule could result in less pronounced effect on the viscosity [51]. The groove binder Hoechst 33258 was used as a reference compound that showed no apparent change in the solution viscosity of ct-DNA. The results indicate a two step binding process in which the Ln(III) complexes

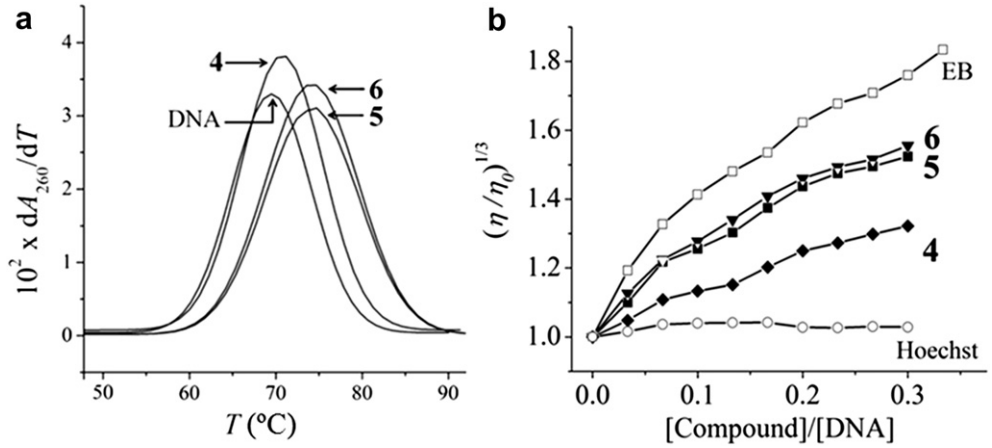

Fig. 4. (a) Derivative plots of dA_{260}/dT vs. T for the thermal denaturation of 180 μM calf thymus DNA alone and on addition of the complexes **4**–**6**. (b) Plots of $(\eta/\eta_0)^{1/3}$ vs. [compound]/[DNA] showing the effect of increasing the concentration of the complexes [Gd(ph-tpy)(acac)$(NO_3)_2$] (**4**, ◆), [Gd(py–tpy)(acac)$(NO_3)_2$] (**5**, ■), [Gd(py–tpy)(sacac)$(NO_3)_2$] (**6**, ▼), ethidium bromide (EB, □) and Hoechst 33258 (○) on the relative viscosities of CT-DNA at 37.0 (±0.1) °C in 5 mM Tris–HCl buffer (pH 7.2) containing 2.5–20% DMF and 180 μM calf thymus DNA.

possibly first interact with the ct-DNA surface followed by groove binding and/or partial intercalation [52].

4.4. Photoinduced DNA cleavage activity

The photo-induced DNA cleavage activity of the complexes **1**–**6** was studied using supercoiled (SC) pUC19 DNA (30 μM, 0.2 μg) in Tris–HCl/NaCl (50 mM, pH, 7.2) buffer by irradiating the samples with a low power monochromatic UV-A light of 365 nm (6 W power). Selected DNA photocleavage data are given in Table 2. The ph–tpy complexes **1** and **4** showed only moderate DNA cleavage activity in UV-A light. The py–tpy complexes with greater DNA binding strength and photosensitizing ability showed efficient photo-induced DNA cleavage activity. The py–tpy complexes showed essentially complete cleavage of SC DNA to its NC form at a complex concentration of 1.0 μM for an exposure time of 1 h (Fig. 5, lanes 8, 9, 11, 12). Control experiment performed with only SC DNA did not show any apparent cleavage of DNA in UV-A light. The ligand py–tpy alone showed ~15% cleavage of SC DNA. The complexes were not cleavage active in dark thus ruling out any possibility of hydrolytic DNA damage (Fig. 5, lane 5). The effect of La(III) vs. Gd(III) metal ion is not apparent from the DNA photocleavage data. The complexes having py–tpy ligand are more active than the ph–tpy complexes. Binding of py-tpy to the Ln(III) thus remarkably enhances its DNA photocleavage activity compared to the ligand or the metal salt alone. The DNA groove binding nature of the complexes was studied using a minor groove binder distamycin-A and a major groove binder methyl green. Distamycin-A and methyl green showed ~15% cleavage of SC DNA in UV-A light. Addition of complex **2** to the distamycin-A bound SC DNA did not inhibit the DNA cleavage activity. Addition of methyl green to complex **2**, however, inhibited the DNA photocleavage activity suggesting DNA major groove binding mode of the py–tpy complexes (Fig. 5) [53]. We also studied the DNA photocleavage activity of the complexes in natural light. The ph–tpy complexes **1** and **4** did not show any significant cleavage activity when treated with DNA and exposed to natural light. A 10 μM solution of the py–tpy complexes **2**, **3**, **5** and **6** showed 40–45% cleavage of SC DNA when irradiated with natural light for 1 h (lanes 18 and 19 in Fig. 5). The moderate photcleavage activity shown by the py–tpy complexes could be a result of photsensitization of the py–tpy moiety by high energy region of the solar spectrum. Therefore, the py–tpy complexes are much less cleavage active in natural light compared to that in UV-A light.

Table 2
Selected DNA cleavage data[a] for the complexes **1**–**6** in UV-A light of 365 nm.

Reaction condition	[Complex] (μM)	t (h)[b]	%NC
DNA control	–	1	2
DNA + **2** (in dark)	1.0	–	10
DNA + py–tpy	1.0	1	15
DNA + **1**	1.0	1	25
DNA + **2**	1.0	1	88
DNA + **3**	1.0	1	81
DNA + **4**	1.0	1	22
DNA + **5**	1.0	1	86
DNA + **6**	1.0	1	78

[a] SC and NC are supercoiled and nicked circular forms of pUC19 DNA (0.2 μg, 30 μM). The DNA cleavage data for the ligands (1.0 μM) and metal salts (1.0 μM) giving %NC for 1 h photoexposure time are: ph–tpy, 7%; Hsacac, 5%; Hacac, 5%; $La(NO_3)_3$, 5% and $Gd(NO_3)_3$, 7%.
[b] Exposure time, t.

4.5. Mechanistic studies

The mechanistic aspects of the UV-A light-induced DNA cleavage activity of the py–tpy complexes were studied using different additives (Fig. 6). The DNA photocleavage reactions involving molecular oxygen could proceed via two major pathways, *viz*., the type-II process forming singlet oxygen ($^1O_2$) or a photoredox pathway forming reactive hydroxyl radicals ($^{\bullet}OH$). Addition of singlet oxygen quenchers, *viz*., sodium azide, TEMP or DABCO to SC DNA showed partial inhibition of the DNA photocleavage activity. Hydroxyl radical scavengers, *viz*., DMSO or catalase also showed partial inhibition in the DNA cleavage activity. The results suggest the formation of both singlet oxygen and hydroxyl radicals as the reactive oxygen species (ROS) responsible for the photodamage of DNA. The singlet oxygen formation was also evidenced from the enhancement of the DNA cleavage activity in D_2O due to longer lifetime of $^1O_2$ in this medium [54]. While the photoactive pyrenyl moiety could generate the singlet oxygen species in a type-II process in UV-A light, the formation of hydroxyl radicals could take place from electron transfer to the oxygen molecule from the photo-excited py–tpy ligand generating radical cation [55]. The photocleavage of DNA at low complex concentration is a significant result in the chemistry of metal-based photochemotherapeutic agents. The presence of heavy lanthanide ion seems to facilitate the

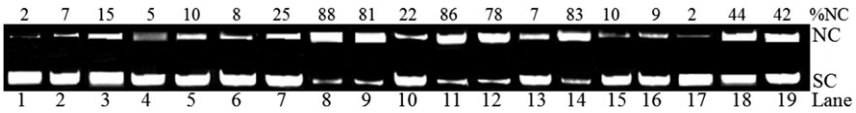

Fig. 5. Gel electrophoresis diagram showing the cleavage of SC pUC19 DNA (0.2 μg, 30 μM) by the complexes (1.0 μM of **1**–**6** in UV-A light and 10 μM of **2, 5** in natural light), the ligands alone (1.0 μM) and the groove binding agents in 50 mM Tris–HCl/NaCl buffer (pH, 7.2) containing 5% DMF on irradiation with UV-A light (lanes 1–16) of 365 nm (6 W) or natural light (lanes 17–19) for 1 h except lanes 5 and 6 that were in dark: lane 1, DNA control; lane 2, DNA + ph–tpy; lane 3, DNA + py–tpy; lane 4, DNA + Hsacac; lane 5, DNA + **1** (in dark lane 6, DNA + **6** (in dark); lane 7, DNA + **1**; lane 8, DNA + **2**; lane 9, DNA + **3**; lane 10, DNA + **4**; lane 11, DNA + **5**; lane 12, DNA + **6**; lane 13, DNA + distamycin-A (50 μM); lane 14, DNA + distamycin-A (50 μM) + **2**; lane 15, DNA + methyl green (200 μM); lane 16, DNA + methyl green (200 μM) + **2**; lane 17, DNA control; lane 18, DNA + **2**; lane 19, DNA + **5**. (For interpretation of the references to colour in this figure legend, the reader is referred to the web version of this article.)

intersystem crossing (ISC) for efficient generation of singlet oxygen and hydroxyl radicals [25,26].

4.6. Cell viability assay

MTT assay was carried out to evaluate the photocytotoxic potential of the complexes **1**–**6** upon photoexcitation on human cervical cancer HeLa cells (Fig. 7). The ph–tpy complexes upon prior incubation for 4 h in the dark and subsequent photoexposure to UV-A light of 365 nm for 15 min showed moderate decrease in the cell viability giving IC_{50} values of 38(±4) μM for **1** and 25(±2) μM for **4** in light and >200 μM for both in dark (Fig. 7(a)). The py–tpy complexes **2**, **3**, **5** and **6** showed a dose-dependent decrease in cell viability with IC_{50} values of 40(±10), 30(±10), 50(±10) and 30(±10) nM, respectively (Fig. 7(b)). The cells unexposed to light exhibited an IC_{50} value of >200 μM for the complexes. The complexes are thus non-toxic in dark but become highly cytotoxic upon photo-irradiation. The pyrenyl ligand is less toxic compared to its complexes giving an IC_{50} value of 70(±10) nM in light while being non-toxic in dark. This observation suggests a more facile intersystem crossing (ISC) mediated by the heavy lanthanides resulting in the generation of singlet oxygen compared to the py–tpy ligand alone [25,26]. No significant difference in the IC_{50} values in light is observed between the pyrenyl complexes bearing carbohydrate appended acac and the acac ligand upon 4 h incubation of the complexes in dark followed by photoexposure. To obtain a deeper insight into the cellular uptake behaviour of the complexes, we carried out time-dependent photocytotoxicity studies using complex **2** having no pendant glucose moiety and complex **3** having a pendant glucose moiety. A 1.0 h incubation of the complexes **2** and **3** in dark followed by photoexposure gave IC_{50} values of 80(±10) and 40(±10) nM, respectively. The IC_{50} values for 2 h incubation of the complexes in the dark followed by photoexposure were 50(±10) nM for **2** and 30(±10) nM for **3**. Therefore, a distinct difference in the IC_{50} values for **2** and **3** is seen at 2 h incubation. Complex **3** bearing a pendant glucose moiety was found to be more cytotoxic compared to the glucose-free complex **2**. The photocytotoxicity of the complexes was found to be very similar for an incubation time of 4 h prior to photoexposure. The results suggest two different cellular uptake pathways for the complexes. The acac complexes being more lipophilic could have a passive

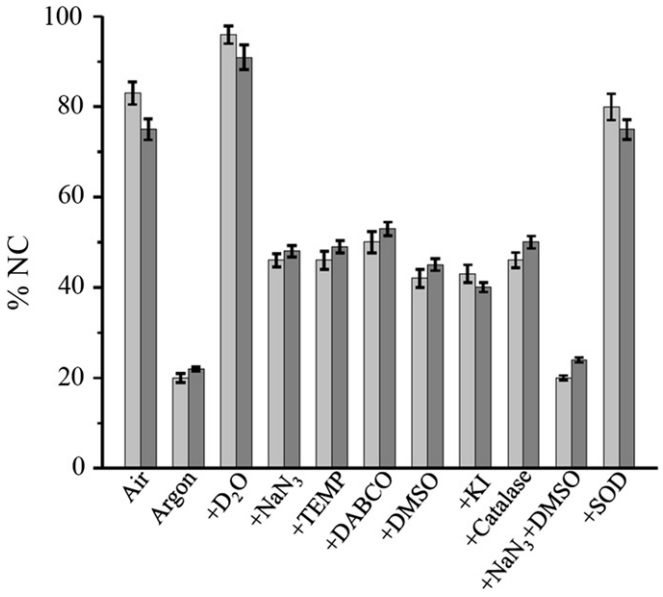

Fig. 6. Bar diagram showing the photocleavage of SC pUC19 DNA (0.2 μg, 30 μM) by [Gd(py–tpy)(acac)$(NO_3)_2$] **(5)** (light shade) and [Gd(py–tpy)(sacac)$(NO_3)_2$] **(6)** (dark shade) in the presence of various additives in Tris–HCl buffer containing 10% DMF. The complex concentration and exposure time are 1.0 μM and 1 h, respectively. The additive concentrations/quantities are: sodium azide, 0.5 mM; KI, 0.5 mM; TEMP, 0.5 mM; DABCO, 0.5 mM; D_2O, 16 μL; DMSO, 4 μL; catalase, 4 units and SOD, 4 units.

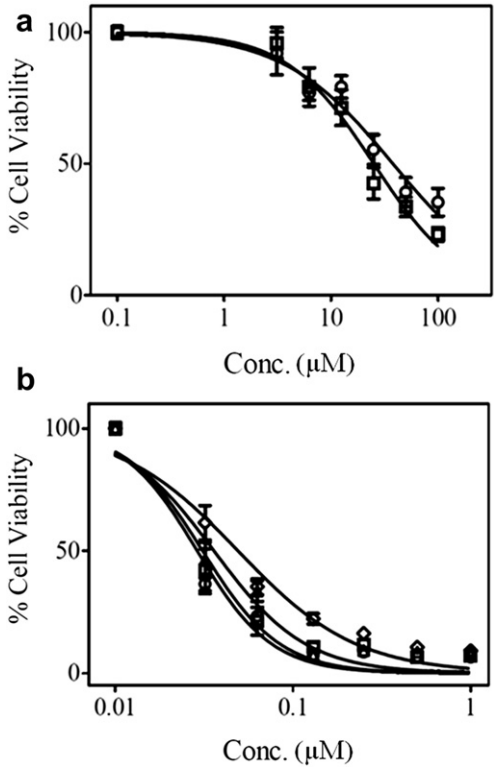

Fig. 7. Cell viability plots showing the photocytotoxicity of the complexes **1** and **4** in panel (a) and **2**, **3**, **5** and **6** in panel (b) In HeLa cells on 4 h incubation in dark followed by exposure to UV-A light of 365 nm (0.55 J cm^{-2}) for 15 min, as determined from the MTT assay. The non-linear fitted curves are shown by circles (○) for complex **1** and squares (□) for complex **4** in panel (a) and the fitted-curves are shown by circles (○) for complex **2**, squares (□) for complex **3**, triangles (△) for complex **5** and diamonds (◇) for complex **6** in panel (b).

diffusion uptake process. The complexes bearing the carbohydrate moiety could have a receptor-mediated endocytic pathway. With reduced lipophilicity of sacac due to the presence of the carbohydrate functionality, the overexpressed glucose transporters (GLUTs) in HeLa cells could be responsible for the endocytosis of the complexes.

We earlier reported the photocytotoxicity of the lanthanide complexes of dipyridophenazine base, *viz*., $[Ln(dppz)_2(NO_3)_3]$ and $[Ln(dppz)(acac)_3]$ in HeLa cells (Table 3) [34,35]. The MTT assay data show that the py–tpy complexes are more photocytotoxic than their ph–tpy or dppz analogues, possibly due to greater photosensitizing ability of the py–tpy ligand. Cisplatin is known to be toxic at an IC_{50} value of 7.5 μM in dark in HeLa cells on 24 h incubation [34]. Incubation of the HeLa cells for 4 h with cisplatin in dark and subsequent photoexposure to UV-A light is known to exhibit IC_{50} values of 71.3 μM in dark and 68.7 μM in UV-A light ($\lambda = 365$ nm) with no apparent PDT effect as expected [34]. Photofrin® with an IC_{50} value of 4.3(±0.2) μM in 633 nm light (5 J cm^{-2} power) and >41 μM in dark in HeLa cells is the FDA approved PDT drug [56]. Complex *trans*-$[Pt(N_3)_2(OH)_2(NH_3)(py)]$ is known to have an IC_{50} value of 6.1(±0.5) μM in UV-A light of 365 nm and >244.3 μM in dark in HaCaT cancer cells [15]. Lanthanide complexes of the py-tpy ligand are thus remarkably photocytotoxic in UV-A light at nanomolar concentrations while remaining essentially non-toxic in dark. The lanthanide complexes are thus potent PDT agents in blue light.

4.7. Photodynamic effect on nuclear morphology

Since the py–tpy complexes showed remarkable photocytotoxicity in UV-A light, we performed fluorescent ethidium bromide-acridine orange (EB/AO) dual staining of the HeLa cells treated with complexes **2** and **3** to understand the mechanism of cell death by monitoring the changes in the nuclear morphology upon PDT (Fig. 8). The cells treated with the complexes in the dark did not show any significant nuclear morphological change. But a significant number of cells treated with the complexes and subsequently photo-irradiated with UV-A light of 365 nm showed apoptotic nuclear morphology. Cell membrane blebbing was seen and the nuclei condensed significantly. The nuclei of the cells treated in dark and the untreated control cells remained intact and stained evenly with AO but not with EB. This difference in staining is because AO is cell-permeable whereas EB is not. In viable cells having an intact plasma membrane, AO crosses the cell membrane and stains the DNA whereas EB is excluded. The cells undergoing apoptosis on treatment with the complex in the presence of light lose membrane integrity during the late stages of apoptosis, cells become permeable to EB and stain orange [57].

Table 3
A comparison of the IC_{50} values of the complexes **1**–**6** with other relevant compounds in HeLa cell.

Compound	IC_{50} in light[a]	IC_{50} in dark[b]
1	38(±4) μM	>200 μM
2	40(±10) nM	>200 μM
3	30(±10) nM	>200 μM
4	25(±2) μM	>200 μM
5	50(±10) nM	>200 μM
6	40(±10) nM	>200 μM
dppz[c]	0.41 μM	11.6 μM
$[Gd(dppz)_2(NO_3)_3]$[c]	0.57 μM	>100 μM
$[Gd(dppz)(acac)_3]$[d]	0.53(±0.03) μM	>100 μM
Photofrin®[e]	4.28(±0.20)[f] μM	>41 μM
Cisplatin	68.7[g] μM	7.5[h] μM

[a] IC_{50} values correspond to 4 h incubation in dark followed by photoexposure to UV-A light of 365 nm (0.55 J cm^{-2}). The respective IC_{50} values for the ph–tpy, py–tpy and Hsacac ligands are 47(±3) μM, 80(±10) nM and >200 μM in UV-A light and >200 μM in dark.
[b] IC_{50} values correspond to 24 h incubation in dark.
[c] The IC_{50} values are taken from Ref.[35].
[d] The IC_{50} values are taken from Ref.[36].
[e] The IC_{50} values are from Ref.[68].
[f] Visible light source of 630 nm.
[g] IC_{50} value of cisplatin in dark for 4 h incubation is 71.3 μM (from Ref.[35]). The value is 68.7 μM after exposure to light.
[h] IC_{50} value on incubation for 24 h in dark. The data from Ref.[35].

4.8. Cellular uptake

The cellular uptake of an anticancer drug is of importance for its effectiveness against tumours [58]. We explored the localization of the complexes inside the HeLa cancer cells from confocal imaging study which was carried out using fluorescent py–tpy complexes **2** and **3** (Fig. 9). Complex **3** having a pendant glucose moiety was used for the confocal study to see the effect of the carbohydrate moiety on the cellular uptake behaviour since GLUT receptors are known to overexpress in a majority of cancer cells and cancer cell lines. There are reports on the overexpression GLUTs, particularly GLUT1, in rapidly growing HeLa cells [59,60]. Confocal studies were carried out using 10 μM solution of the complexes with propidium iodide (PI) as a nuclear staining agent which also served as a reference. The confocal images were taken after 15 min, 30 min, 1 h and 4 h of incubation of the complexes to see their time-dependent uptake and localization inside the cells. The images taken after 15 min showed little uptake of both the complexes as seen from the intracellular fluorescence intensity seen in the cells in panels (a), (b) and (c) in Figs. 9 and 10. Images taken after 30 min showed no significant enhancement in the fluorescence intensities for both the complexes (panels (d), (e) and (f) in Figs. 9 and 10). Interestingly, images of the cells treated with the glucose-bearing complex **3** collected after 1 h showed remarkable enhancement in intensity having diffused cytosolic distribution with punctate staining of the cells around the perinuclear region (panels (g), (h) and (i) in Fig. 10). The images were found to be of much less intensity for glucose-free complex **2** (panels (g), (h) and (i) in Fig. 9). However, the confocal images of the cells taken after 4 h showed similar intensity pattern for both the complexes (panels (j), (k) and (l) in Figs. 9 and 10). The intracellular localization of complex **2** did not show any granular appearance, but largely a diffused staining of the whole cytoplasm. The nucleus gave little or no blue emission, indicative of negligible nuclear uptake in both the cases. These observations suggest two possible cellular uptake pathways for the glucose-free complex **2** taken up by a diffusion process and the glucose-bearing complex **3** internalized by receptor-mediated endocytosis (RME). The observation of similar punctate staining of cells treated with the metal complex bearing a pendant glucose moiety has been reported in the literature [60]. No change in the nuclear morphology was seen in the confocal images of the cells indicating the fact that the complexes remain harmless in the dark but show potent PDT effect upon photoexposure. The results are indeed interesting considering that the present complexes could serve the dual purpose of detecting the tumour and damaging the DNA upon photoactivation leading to apoptosis. The lanthanide-based MRI agents are only useful for tumour detection but not for its selective damage.

5. Conclusions

The photo-induced DNA cleavage activity and photocytotoxicity of six lanthanide complexes having tridentate *N,N,N*-donor terpyridine and acetylacetonate ligands are presented. The La(III) and Gd(III) complexes show $LnO_{6(7)}N_3$ core in the solid state and LnO_4N_3 core in a solution phase. The py–tpy complexes with

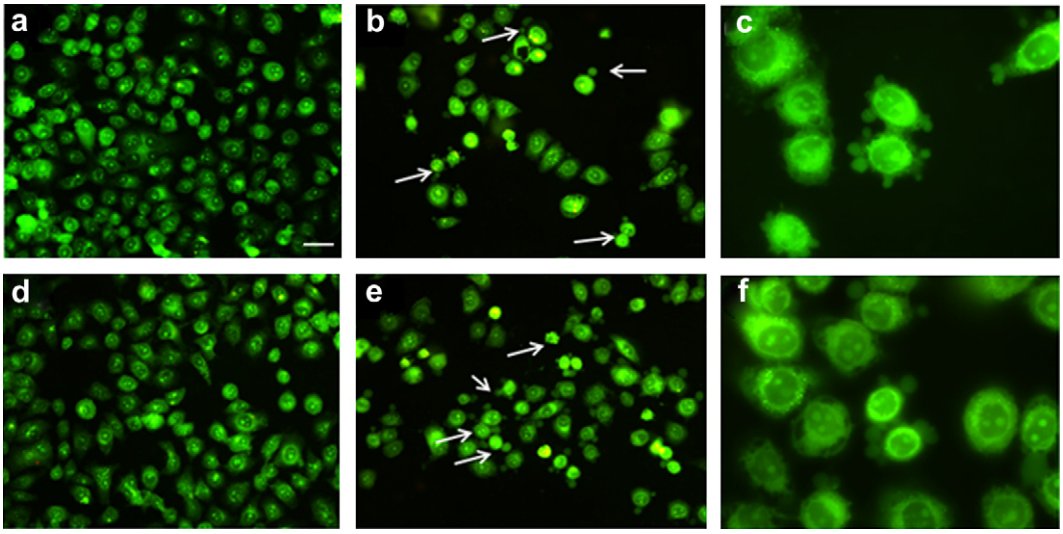

Fig. 8. Ethidium bromide/acridine orange staining of HeLa cells treated with complex **2** (50 nM) and complex **3** (50 nM) to identify nuclear morphology. Panels (a) and (d) correspond to the cells treated with respective complex **2** and **3** in dark, panels (b) and (e) correspond to the cells treated with respective complex **2** and **3** and irradiated with UV-A light of 365 nm (0.55 J cm^{-2}) showing significant apoptosis of the cells and panels (c) and (f) correspond to the cells in panels (b) and (e) respectively visualized at 63× magnification showing the membrane blebbing of the apoptotic cells. The scale bar corresponds to 10 μm. (For interpretation of the references to colour in this figure legend, the reader is referred to the web version of this article.)

a planar pyrenyl moiety show intercalative DNA binding propensity. The py–tpy complexes with the photoactive pyrenyl moiety display efficient UV-A light-induced DNA cleavage activity at low complex concentration via mechanistic pathways that involve formation of both singlet oxygen and hydroxyl radicals. The DNA photocleavage observed at only 1.0 μM complex concentration is significant towards using lanthanide-based complexes as synthetic photonucleases. The complexes do not show any apparent DNA hydrolytic cleavage activity thus making them suitable for potential photoactivated chemotherapeutic applications. The py–tpy complexes display remarkable photocytotoxic effect in HeLa cells giving IC_{50} values in the nanomolar range and a time-dependent photocytotoxicity is observed for the complexes. The EB/AO dual staining of the HeLa cells treated with complexes **2** and **3** shows apoptosis as the major pathway of the cell death. The confocal fluorescence microscopy of HeLa cells using the py–tpy complexes **2** and **3** reveals localization of the complex primarily in the cytosol of the HeLa cells. The uptake of the py–tpy complexes **3** and **6** having an appended glucose moiety seems to be endocytosis mediated by overexpressed GLUTs in the HeLa cells. Interestingly, the complexes are non-toxic in dark but become highly cytotoxic on photoactivation. With significant PDT effect at nanomolar complex concentration range, the present py–tpy lanthanide complexes could serve dual purpose of detecting the tumour while remaining dormant inside the cell in dark till subjected to photoactivation causing apoptotic cellular death selectively at the photo-exposed cells leaving unexposed healthy cells unaffected. In contrast, the lanthanide-based MRI agents are useful for only tumour detection but not for tumour damage. The present results are indeed encouraging and are likely to presage designing and developing new lanthanide complexes as potent photochemotherapeutic and tumour imaging agents.

6. Experimental protocols

6.1. Materials

All reagents and chemicals were purchased from commercial sources (S.D. Fine Chemicals, India; Sigma–Aldrich, U.S.A.) and used without further purifications. Solvents were purified by standard procedures [61]. Supercoiled (SC) pUC19 DNA (caesium chloride purified) was purchased from Bangalore Genie (India). Tris-(hydroxymethyl)aminomethane-HCl (Tris–HCl) buffer (pH = 7.2) was prepared using deionized and sonicated triple distilled water. Calf thymus DNA, agarose (molecular biology grade), distamycin-A, methyl green, catalase, SOD, TEMP, DABCO, EB, PI and MTT were purchased from Sigma (U.S.A.). The terpyridine derivatives, *viz*., 4′-phenyl-2,2′:6′,2″-terpyridine (ph–tpy) and 4′-(1-pyrenyl)-2,2′:6′,2″-terpyridine (py–tpy) were prepared following published procedures [39,40]. The carbohydrate-appended ligand, 4-hydroxy-6-{4-[(β-D-glucopyranoside)oxy]phenyl}hex-3,5-dien-2-one (Hsacac), was prepared according to a literature method [41].

6.2. Instrumentation

The elemental analyses were done using a Thermo Finnigan Flash EA 1112 CHNS analyzer. The infrared spectra were recorded on a Bruker ALPHA FT-IR spectrometer. Electronic spectra were recorded on a PerkinElmer Lambda 650 UVvis spectrometer. Molar conductivity measurements were performed using a Control Dynamics (India) conductivity metre. Room temperature magnetic susceptibilities of the DMSO-d_6 solutions of the Gd(III) complexes containing 1% TMS (v/v) as the internal reference were obtained by a solution NMR method with a Bruker AMX-400 NMR spectrometer [62,63]. The magnetic moments were calculated by Evans method using the equation: $\mu_{eff} = 0.0618(\Delta f T/f M)$, where Δf is the observed shift in frequency of the TMS signal, T is the temperature (K), f is the operating frequency (MHz) of the NMR spectrometer, and M is the molarity of the complex in the solution. Electrospray ionization mass spectral (ESI-MS) measurements were carried out using Bruker Daltonics make Esquire 300 Plus ESI Model instrument. ^{1}H-NMR spectra of the diamagnetic La(III) complexes were recorded at room temperature on a Bruker 400 MHz NMR spectrometer. Room temperature fluorescence quantum yield measurements were done using a PerkinElmer LS 55 fluorescence spectrometer using pure anthracene as a standard [64]. Photobleaching experiments were carried out using a PerkinElmer LS 55 fluorescence spectrometer by monitoring the

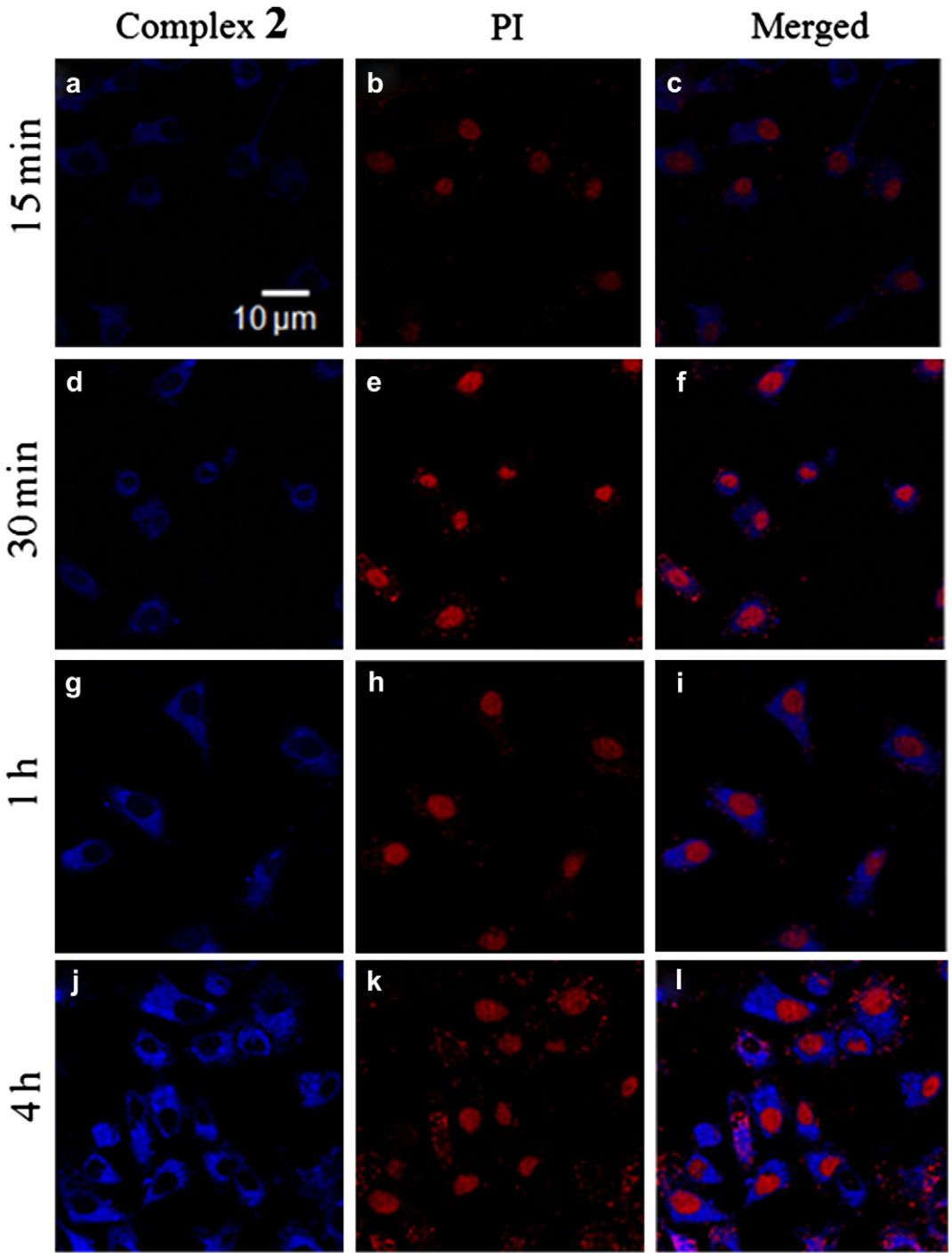

Fig. 9. A time-course collection of confocal microscopic images of the HeLa cells treated with [La(py–tpy)(acac)$(NO_3)_2$](**2**, 10 μM) and propidium iodide (PI). Panels (a), (d), (g) and (j) correspond to the blue emission of complex **2** upon excitation at 365 nm and the respective images were taken after 15 min, 30 min, 1 h and 4 h. Panels (b), (e), (h) and (k) correspond to the red emission of PI. Panels (c), (f), (i) and (l) are the merged images of the first two panels. The scale bar corresponds to 10 μm. (For interpretation of the references to colour in this figure legend, the reader is referred to the web version of this article.)

change in the emission intensity of the py–tpy complexes after irradiation of a 10 μM solution of the complex in aqueous DMSO (1:4 v/v) with UV-A light of 365 nm (UV lamp, 100 W). The room temperature emission spectra were recorded at an interval of 5 min post-irradiation upto a total duration of 60 min. The test solutions were continuously stirred during the experiment to ensure homogeneous bleaching (if any). The emission signals due to the py–tpy chromophore were recorded (excitation wavelength, 350 nm). Fluorescence microscopic investigations were carried out on Leica DM IL microscope with integrated Leica DFC400 camera and IL50 image software. Confocal microscopy was done using confocal scanning electron microscope (Leica, TCS SP5 DM6000).

6.3. Synthesis of the complexes ***1–6***

The complexes were prepared by following a general synthetic method. An ethanol solution (15 ml) of $Ln(NO_3)_3.6H_2O$ (0.43 g for

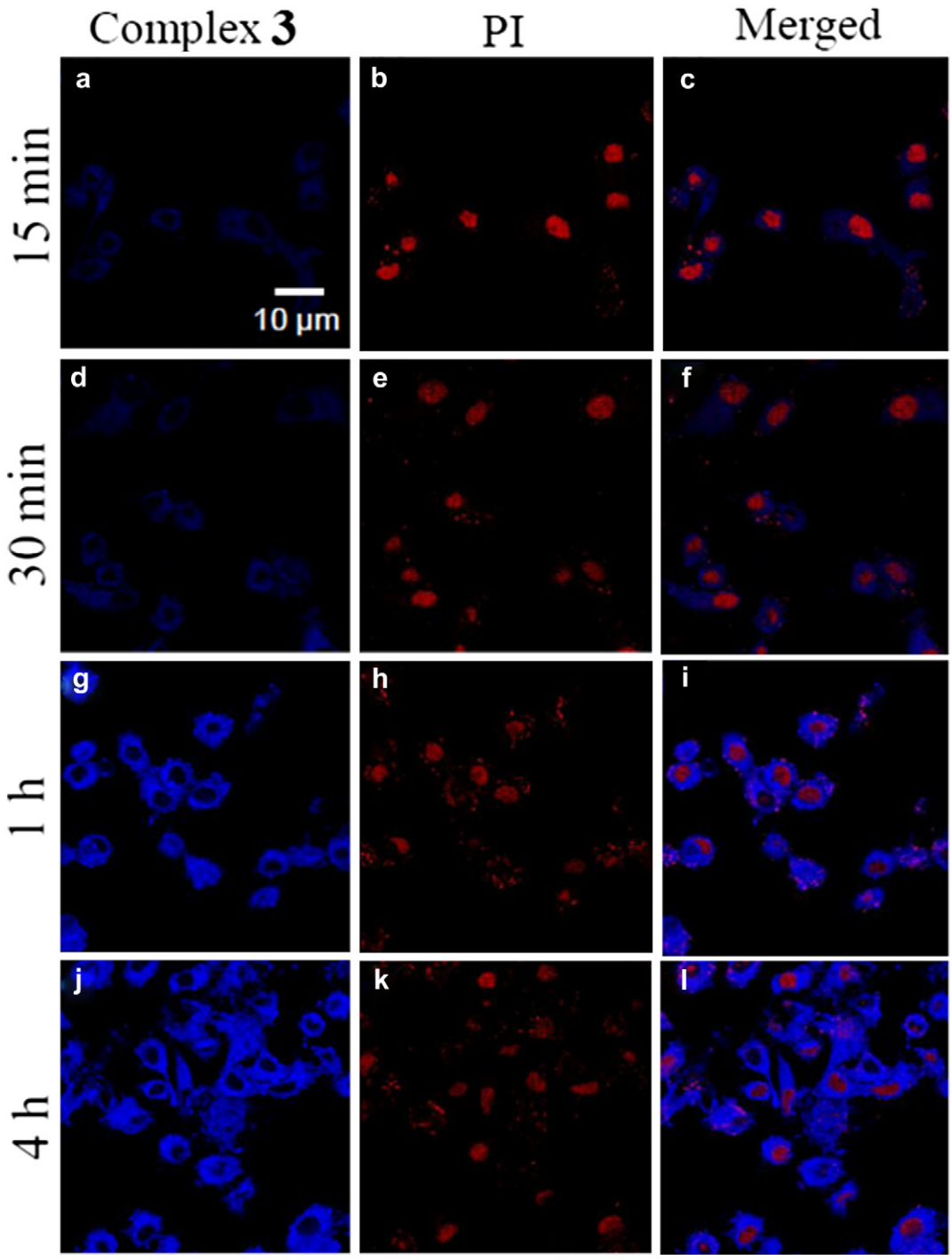

Fig. 10. A time-course collection of confocal microscopic images of the HeLa cells treated with [La(py–tpy)(sacac)$(NO_3)_2$](**3**, 10 μM) and propidium iodide (PI). Panels (a), (d), (g) and (j) correspond to the blue emission of complex **3** upon excitation at 365 nm and the respective images were taken after 15 min, 30 min, 1 h and 4 h. Panels (b), (e), (h) and (k) correspond to the red emission of PI. Panels (c), (f), (i) and (l) are the merged images of the first two panels. The scale bar corresponds to 10 μm. (For interpretation of the references to colour in this figure legend, the reader is referred to the web version of this article.)

La(III) and 0.45 g for Gd(III), 1.0 mmol) was added dropwise to a dichloromethane solution (15 ml) of the terpyridine ligand (ph–tpy, 0.31 g; py–tpy, 0.44 g; 1.0 mmol) with stirring for 1 h at 25 °C. The reaction mixture was cooled to 0 °C to afford a crystalline solid of [Ln(ph–tpy)$(NO_3)_3$] or [Ln(py–tpy)$(NO_3)_3$] as the precursor complex which was filtered, washed with ice-cold ethanol followed by diethyl ether and finally dried in vacuum and used directly in the next step.

To an ethanol suspension (15 ml) of the precursor complex [Ln(phtpy)$(NO_3)_3$] (0.32 g, La(III); 0.33 g, Gd(III), 0.5 mmol) or [Ln(py–tpy)$(NO_3)_3$] (0.38 g, La(III); 0.39 g, Gd(III), 0.5 mmol) was added the β-diketone ligand (0.15 g, Hacac; 0.55 g, Hsacac, 1.5 mmol) dissolved in methanol (15 ml) and the pH of the reaction mixture was adjusted to 7.5 using triethylamine. After 1h of stirring at room temperature, a clear solution was obtained which was further stirred for 2 h and filtered. Slow evaporation of the solution

gave a crystalline solid of the desired product which was isolated and washed with cold methanol followed by diethyl ether and finally dried in vacuum over P_4O_{10} (Yield: ~70%). The characterization data for the complexes are given below.

*6.3.1. [La(ph–tpy)(acac)(NO$_3$)$_2$] (**1**)*

Anal. calc. for $C_{26}H_{22}N_5O_8La$: C, 46.51; H, 3.30; N, 10.43. Found: C, 46.65; H, 3.50; N, 10.38%. ESI–MS in 20% aqueous MeOH (*m*/*z*): 609.10 [M-(NO_3^-)]$^+$. FT–IR, cm^{-1}: 3065 *w*, 1595 vs, 1572 m, 1512 s, 1450 s, 1415 s, 1378 s, 1351 m, 1290 s, 1263 m, 1165 m, 1074 *w*, 1028 m, 1010 s, 922 *w*, 880 *w*, 840 m, 815 *w*, 790 m, 764 s, 732 m, 691 m, 658 *w*, 635 m, 617 m, 533 *w*, 497 *w*, 410 w (vs, very strong; s, strong; m, medium; *w*, weak). UV–visible in DMF [λ_{max}, nm (ε, M^{-1} cm^{-1})]: 310sh (15,670), 278 (38,680) (sh, shoulder). ^{1}H NMR in DMSO-d_6 (δ, ppm): 8.80 (d, 2H, J = 4.5 Hz), 8.72 (s, 2H), 8.68 (d, 2H, J = 8.2 Hz), 8.15 (d, 2H, J = 8.0 Hz), 7.92 (d, 2H, J = 7.5 Hz), 7.50–7.65 (m, 5H), 5.40 (s, 1H), 1.80 (s, 6H) (s, singlet; d, doublet; m, multiplet). Molar conductance (Λ_M) in 1:5 aqueous DMF at 298 K : 101 S cm^2 M^{-1}.

*6.3.2. [La(py–tpy)(acac)(NO$_3$)$_2$] (**2**)*

Anal. calc. for $C_{36}H_{26}N_5O_8La$: C, 54.35; H, 3.29; N, 8.80. Found: C, 54.50; H, 3.33; N, 8.75%. ESI–MS in 10% aqueous MeOH (*m*/*z*): 733.50 [M-(NO_3^-)]$^+$. FT–IR, cm^{-1}: 3050 *w*, 1580 s, 1560 m,1515 m, 1460 s, 1435 s, 1410 s, 1389 m, 1293 s, 1187 *w*, 1086 *w*, 1041 *w*, 1005 m, 893 *w*, 840 s, 780 m, 737 m, 720 m, 683 m, 658 *w*, 625 m, 580 *w*, 560 *w*, 507 *w*, 475 *w*, 462 *w*, 415 w. UV–visible in DMF [λ_{max}, nm (ε, M^{-1} cm^{-1})]: 350 (45,790), 331 (34,320), 315 (19,940), 278 (78,250), 268 (64,830). ^{1}H NMR in DMSO-d_6 (δ, ppm): 8.98 (s, 2H), 8.77 (d, 2H, J = 7.7 Hz), 8.58 (d, 2H, J = 4.6 Hz), 8.50–8.25 (m, 8H), 8.11 (t, 1H, J = 7.9 Hz), 7.95 (m, 2H), 7.70 (m, 2H), 5.5 (s, 1H), 1.78 (s, 6H). Molar conductance (Λ_M) in 1:5 aqueous DMF at 298 K: 108 S cm^2 M^{-1}.

*6.3.3. [La(py–tpy)(sacac)(NO$_3$)$_2$] (**3**)*

Anal. calc. for $C_{49}H_{40}N_5O_{14}La$: C, 55.43; H, 3.80; N, 6.60. Found: C, 55.50; H, 3.92; N, 6.67%. ESI–MS in 10% aqueous MeOH (*m*/*z*): 999.11 [M-(NO_3^-)]$^+$. FT–IR, cm^{-1}: 3312s, 3060 *w*, 1581 vs, 1566 s, 1510 s, 1465 m, 1389 s, 1233 s, 1176 m, 1070 m, 1040 m, 1018 m, 989 m, 893 *w*, 843 s, 790 *w*, 780 *w*, 755 *w*, 740 *w*, 720 *w*, 681w, 660 m, 623 *w*, 588 *w*, 558w, 540 *w*, 517 *w*, 474 *w*, 458 *w*, 426 w. UV–visible in DMF [λ_{max}, nm (ε, M^{-1} cm^{-1})]: 350 (57,730), 278 (45,280). ^{1}H NMR in DMSO-d_6 (δ, ppm): 9.01 (s, 2H, J = 8.5 Hz), 8.80 (d, 2H, J = 7.8 Hz), 8.61 (d, 2H, J = 4.4 Hz), 8.48–8.20 (m, 8H), 7.90 (t, 1H, J = 7.9 Hz), 7.72 (m, 2H), 7.65 (d, 1H, J = 15.1 Hz), 7.50 (m, 2H), 7.40–7.28 (m, 4H), 6.52 (d, 1H, J = 15.1 Hz), 5.72 (s, 1H), 4.96 (d, 1H, J = 7.8 Hz), 4.81(m, 1H, J = 7.1, 6.8 Hz), 4.72 (m, 1H), 4.58 (m, 1H), 4.35 (m, 1H), 4.26 (m, 1H), 3.85 (m, 1H), 2.15 (s, 3H). Molar conductance (Λ_M) in 1:5 aqueous DMF at 298 K: 110 S cm^2 M^{-1}.

*6.3.4. [Gd(ph–tpy)(acac)(NO$_3$)$_2$] (**4**)*

Anal. calc. for $C_{26}H_{22}N_5O_8Gd$: C, 45.28; H, 3.21; N, 10.15. Found: C, 45.40; H, 3.33; N, 10.25%. ESI–MS in 20% aqueous MeOH (*m*/*z*): 628.15 [M-(NO_3^-)]$^+$. FT–IR, cm^{-1}: 3040 *w*, 1590 vs, 1572 *w*, 1520 s, 1460 vs, 1410 m, 1380 s, 1282 s, 1262 m, 1160 m, 1076 *w*, 1030 m, 1006 s, 925 m, 894 *w*, 850 *w*, 820 *w*, 795 m, 765 s, 735 m, 695 m, 660 *w*, 635 *w*, 620 m, 533 *w*, 498 *w*, 422 w. UV–visible in DMF [λ_{max}, nm (ε, M^{-1} cm^{-1})]: 309sh (15,830), 280 (39,050). μ_{eff} = 8.01 μ_B at 298 K. Molar conductance (Λ_M) in 1:5 aqueous DMF at 298 K: 105 S cm^2 M^{-1}.

*6.3.5. [Gd(py–tpy)(acac)(NO$_3$)$_2$] (**5**)*

Anal. calc. for $C_{36}H_{26}N_5O_8Gd$: C, 53.13; H, 3.22; N, 8.60. Found: C, 53.31; H, 3.34; N, 8.68%. ESI–MS in 10% aqueous MeOH (*m*/*z*): 752.05 [M-(NO_3^-)]$^+$. IR data, cm^{-1}: 3065 *w*, 1581 s, 1560 s, 1505 s, 1470 m, 1430 m, 1415 m, 1389 s, 1280 m, 1183 m, 1072 s, 1040 m, 1015 m, 893 *w*, 841 s, 795 m, 773 *w*, 757 *w*, 742 m, 716 m, 683 *w*, 661 *w*, 628 m, 590 *w*, 560 *w*, 540 *w*, 521 *w*, 482 *w*, 460 *w*, 421 w. UV–visible in DMF [λ_{max}, nm (ε, M^{-1} cm^{-1})]: 350 (48,060), 331 (36,930), 316 (21,200), 278 (70,020), 265 (62,060). μ_{eff} = 7.98 μ_B at 298 K. Molar conductance (Λ_M) in 1:5 aqueous DMF at 298 K: 103 S cm^2 M^{-1}.

*6.3.6. [Gd(py–tpy)(sacac)(NO$_3$)$_2$] (**6**)*

Anal. calc. for $C_{49}H_{40}N_5O_{14}Gd$: C, 55.49; H, 3.73; N, 6.48. Found: C, 55.69; H, 3.65; N, 6.62%. ESI–MS in 10% aqueous MeOH (*m*/*z*): 1018.33 [M-(NO_3^-)]$^+$. IR data, cm^{-1}: 3312 s, 3045 *w*, 1584 vs, 1565 s, 1508 s, 1470 m, 1390 s, 1231 s, 1175 m, 1067 m, 1040 m, 1012 m, 989 m, 896 *w*, 840 s, 790 m, 783 *w*, 760 *w*, 744 m, 722 *w*, 678 *w*, 660 *w*, 620 *w*, 590 *w*, 557 m, 537 *w*, 476 *w*, 456 *w*, 420 w. UV–visible in DMF [λ_{max}, nm (ε, M^{-1} cm^{-1})]: 350 (57,600), 280 (53,800). μ_{eff} = 8.05 μ_B at 298 K. Molar conductance (Λ_M) in 1:5 aqueous DMF at 298 K: 95 S cm^2 M^{-1}.

6.4. Solubility and stability

All the complexes showed good solubility in DMF and DMSO and moderate solubility in methanol, ethanol and acetonitrile. Complexes **3** and **6** were moderately soluble in water but showed poor solubility in chlorinated solvents due to the presence of a carbohydrate moiety. The complexes were found to be stable in the monocationic form due to dissociation of the nitrate anion and the solution stability of the cationic species was ascertained from the ESI-MS as well as from the molar conductivity data.

6.5. X-ray crystallographic procedure

The crystal structures of the complexes **1** as [La(ph–tpy)(acac)(EtOH)(NO$_3$)$_2$] (**1a**) and **4** were obtained by single crystal X-ray diffraction method. Single crystals of **1a** were grown by slow evaporation of a solution of the complex in EtOH-MeOH mixture (1:1 v/v). The single crystals of **4** were obtained by vapour diffusion of diethyl ether into a methanol solution of the complex. Crystal mounting was done on glass fibre with epoxy cement. All geometric and intensity data were collected at room temperature using an automated Bruker SMART APEX CCD diffractometer equipped with a fine focus 1.75 kW sealed tube Mo-K$_\alpha$ X-ray source (λ = 0.71073 Å) with increasing ω (width of 0.3° per frame) at a scan speed of 8 s per frame for complex **1a** and 5 s per frame for complex **4**. Intensity data, collected using ω-2θ scan mode, were corrected for Lorentz–polarization effects and for absorption [65]. The structures were solved by a combination of Patterson and Fourier techniques and refined by full-matrix least-squares method using SHELX system of programs [66]. All hydrogen atoms belonging to the complexes were refined using a riding model. All non-hydrogen atoms were refined anisotropically. Perspective views of the molecules were obtained by ORTEP [67]. The CCDC numbers for the complexes **1a** and **4** are 844349 and 844350, respectively.

Crystal data for **1a**: $C_{28}H_{27}LaN_5O_9$, M = 716.46, triclinic, space group $P\bar{1}$, a = 8.3959(3); b = 10.1193(3); c = 18.0790(6) Å, α = 95.588(2), β = 100.109(2), γ = 101.898(2)°, V = 1465.38(8) Å^3, Z = 2, D_c = 1.522 Mg m^{-3}, T = 293(2) K, 30.53 ≥ θ ≥ 2.08°, μ = 1.511 cm^{-1}, F(000) = 668, GOF = 0.997, R_1 = 0.0469, wR_2 = 0.0958 for 8730 reflections with $I > 2\sigma(I)$ and 388 parameters [R_1 (F^2) = 0.074 (all data)]. Weighting scheme: $w = [\sigma^2(F_o)^2 + (0.0412\ P)^2 + 0.0000\ P]^{-1}$, where $P = (F_o^2 + 2F_c^2)/3$.

Crystal data for **4**: $C_{26}H_{22}GdN_5O_8$, M = 689.74, triclinic, space group $P\bar{1}$, a = 9.4899(6); b = 10.8580(8); c = 14.1264(10) Å, α = 77.276(4), β = 81.896(4), γ = 69.773(4)°, V = 1328.95(16) Å^3, Z = 2, D_c = 1.724 Mg m^{-3}, T = 293(2) K, 30.46 ≥ θ ≥ 1.48°, μ = 2.554 cm^{-1}, F(000) = 682, GOF = 1.039, R_1 = 0.035,

wR_2 = 0.075 for 7843 reflections with $I > 2\sigma(I)$ and 361 parameters [R_1 (F^2) = 0.059 (all data)]. Weighting scheme: $w = [\sigma^2(F_o)^2 + (0.0313P)^2 + 0.0000P]^{-1}$, where $P = (F_o^2 + 2F_c^2)/3$.

6.6. Pharmacological evaluations

6.6.1. DNA binding studies

6.6.1.1. Electronic absorption spectroscopy. DNA binding studies were carried out in Tris–HCl/NaCl buffer (5 mM Tris–HCl, 5 mM NaCl, pH 7.2) using DMF solutions of the complexes **1**–**6**. Calf thymus DNA (ca. 350 μM NP) in this buffer medium gave a ratio of ca. 1.9:1 of the UV absorbance at 260 and 280 nm indicating the DNA apparently free from protein impurities. The DNA concentration was estimated from its absorption intensity at 260 nm with a known molar extinction coefficient (ε) value of 6600 M^{-1} cm^{-1} [68]. Absorption titration experiments were made by varying the concentration of the DNA while keeping the complex concentration constant. Due correction was made for the absorbance of DNA itself. Each spectrum was recorded after equilibration of the sample for 5 min. The intrinsic equilibrium binding constant (K_b) and the fitting parameter (s) of the complexes **1**–**6** to DNA were obtained by McGhee-von Hippel (MvH) method using the expression of Bard et al. by monitoring the change of the absorption intensity of the spectral bands with increasing concentration of calf thymus DNA by regression analysis using equation: $(\varepsilon_a - \varepsilon_f)/(\varepsilon_b - \varepsilon_f) = (b - (b^2 - 2K_b^2C_t[DNA]_t/s)^{1/2})/2K_bC_t$, where $b = 1 + K_bC_t + K_b[DNA]_t/2s$ and ε_a is the extinction coefficient observed for the absorption band at a given DNA concentration, ε_f is the extinction coefficient of the complex free in solution, ε_b is the extinction coefficient of the complex when fully bound to DNA, K_b is the equilibrium binding constant, C_t is the total metal complex concentration, $[DNA]_t$ is the DNA concentration in nucleotides and s is the fitting parameter for the MvH equation giving an estimate of the binding site size in base pairs [69,70]. The non-linear least-squares analyses were done using Origin Lab, version 8.1.

6.6.1.2. DNA melting experiments. DNA melting experiments were carried out by monitoring the absorbance of the ct-DNA (180 μM) at 260 nm at various temperatures, both in the absence and presence of the complexes. Measurements were carried out using a PerkinElmer Lambda 650 UV/VIS spectrometer with a PTP-1+1 Peltier temperature controller at an increase rate of 0.5 °C per min.

6.6.1.3. Viscosity experiments. Viscometric titrations were performed with a Schott Gerate AVS 310 Automated Viscometer thermostated at 37 °C in a constant temperature bath. The concentration of ct-DNA was 150 μM in NP (nucleotide pair) and the flow times were measured using an automated timer. Each sample was measured 3 times and an average flow time was calculated. Plots of $(\eta/\eta_0)^{1/3}$ vs. [compound]/[DNA] were made, where η is the viscosity of the DNA solution in the presence of the compound and η_0 is that of the DNA solution alone. Viscosity values were calculated from the observed flow time of the DNA-containing solutions (t) corrected for that of the buffer alone (t_0), $\eta = (t - t_0)/t_0$. Due corrections were made for the viscosity of DMF solvent present in the aqueous buffer solution of DNA.

6.6.2. DNA cleavage experiments

The cleavage of supercoiled (SC) pUC19 DNA (30 μM, 0.2 μg, 2686 base-pairs) was studied by agarose gel electrophoresis. For photo-induced DNA cleavage studies, the reactions were carried out under illuminated conditions using UV-A light of 365 nm (6 W, Model LF-206.LS of Bangalore Genei). Eppendorf vials were used for photocleavage experiments in a dark room at 25 °C using SC DNA (1.0 μL, 30 μM) in 50 mM Tris–HCl buffer (pH 7.2) containing 50 mM NaCl and the complex (2.0 μL) with varying concentrations. The concentration of the complexes in DMF or the additives in buffer corresponded to the quantity in 2.0 μL stock solution after dilution to the 20 μL final volume using Tris–HCl buffer. The solution path length in the sample vial was ~5 mm. After light exposure, each sample was incubated for 1.0 h at 37 °C and analyzed for the photo-cleaved products using gel electrophoresis. Experiments to study the groove binding selectivity of the complexes were carried out in the presence of distamycin (50 μM) and methyl green (200 μM) as the DNA minor and major groove binder, respectively [71,72]. The SC DNA was pre-treated with distamycin or methyl green and then treated with the complex as described above. Mechanistic studies were done using different additives (NaN_3, 0.5 mM; TEMP, 0.5 mM; DABCO, 0.5 mM; DMSO, 4 μL; KI, 0.5 mM; catalase, 4 units; SOD, 4 units) prior to the addition of the lanthanide complex. For the D_2O experiment, this solvent was used for dilution of the sample to 20 μL sample volume. The samples after incubation in a dark room were added to the loading buffer containing 0.25% bromophenol blue, 0.25% xylene cyanol, 30% glycerol (3.0 μL) and the solution was finally loaded on 1% agarose gel containing 1.0 μg ml^{-1} ethidium bromide (EB). Electrophoresis was done in a dark room for 2.0 h at 60 V in TAE (Tris-acetate EDTA) buffer. Bands were visualized in UV light and photographed. The extent of SC DNA cleavage was estimated from the intensities of the bands using UVITEC Gel Documentation System. Due corrections were made for the low level of nicked circular (NC) form of DNA present in the original SC DNA sample and for low affinity of EB binding to SC compared to NC form of DNA [73]. The observed error in measuring the gel band intensities was in the range of 3–5%.

6.6.3. Cell culture

HeLa (human cervical carcinoma) cells were maintained in DMEM supplemented with 10% FBS, 100 IU ml^{-1} of penicillin, 100 μg ml^{-1} of streptomycin and 2 mM of Glutamax at 37 °C in a humidified incubator at 5% CO_2. The adherent cultures were grown as monolayer and were passaged once in 4–5 days by treatment with 0.25% Trypsin-EDTA.

6.6.4. Photocytotoxicity experiments

Photocytotoxicity of the complexes **1**–**6** was studied using MTT assay which is based on the ability of mitochondrial dehydrogenases of viable cells to cleave the tetrazolium rings of MTT forming dark purple membrane impermeable crystals of formazan that could be measured at 540 nm after solubilization in DMSO [42]. Approximately, 10^4 HeLa cells in a 96-well culture plate in DMEM containing 10% FBS were incubated for 24 h at 37 °C in a CO_2 incubator, followed by addition of the complex solution in a medium containing 1% DMSO. After 4 h of incubation in dark, the medium was replaced with phosphate buffered saline (PBS) and the culture plate was exposed to UV-A light of 365 nm (6 W). PBS was replaced with fresh medium, and cells were further incubated for 24 h in the dark. Finally, a 25 μL of 4 mg ml^{-1} of MTT was added to each well and again incubated for an additional 3 h. After discarding the culture medium, 200 μL of DMSO was added to dissolve the formazan crystals formed, and the absorbance at 540 nm was measured using a BIORAD ELISA plate reader. The cytotoxicity was measured from the absorbance ratio of the treated cells and untreated controls. The IC_{50} values were determined by non-linear regression analysis using GraphPad Prism software.

6.6.5. Nuclear staining experiments

HeLa cells cultured on cover-slips were photo-irradiated with a UV-A light of 365 nm (6 W) following 4 h of incubation in the dark in the presence of 50 nM of the complexes **2** and **3**. The cells were

then allowed to recover for 1 h, washed three times with PBS and stained with an EB/AO mixture (1:1, 10 μM) for 15 min and observed at 20× magnification with a fluorescence microscope [20].

6.6.6. Confocal microscopy

HeLa cells (4 x 10^4 cells/mm^2) plated on cover slips, were incubated with 10 μM of the complexes **2** and **3** for different time intervals of 15 min, 30 min, 1 h and 4 h in dark, fixed with 4% paraformaldehyde for 10 min at 25 °C and washed with PBS. This was followed by incubation with propidium iodide (PI) staining solution for 1.0 h at 42 °C. The cells were washed free of excess PI and mounted. Images were acquired using the confocal scanning microscope (Leica, TCS SP5 DM6000) and analysed using the LAS AF Lite software.

Acknowledgements

We thank the Department of Science and Technology (DST), Government of India, for financial support (SR/S5/MBD-02/2007). We are thankful to DST for a CCD diffractometer facility and the Department of Biotechnology for the imaging facility. A.R.C. thanks the DST for J. C. Bose national fellowship. A.H., S.G. and T.K.G. thank the Council of Scientific and Industrial Research (CSIR), New Delhi, for research fellowships. The authors thank IRIS, IISc and P. Janardhan for assistance with the confocal fluorescence microscopy experiments.

Appendix. Supplementary material

Supplementary data associated with this article can be found, in the online version, at doi:10.1016/j.ejmech.2012.02.011.

References

[1] N.J. Farrer, L. Salassa, P.J. Sadler, Dalton Trans. (2009) 10690–10701.
[2] H.T. Chifotides, K.R. Dunbar, Acc. Chem. Res. 38 (2005) 146–156.
[3] (a) N.L. Fry, P.K. Mascharak, Acc. Chem. Res. 44 (2011) 289–298;
(b) A.D. Ostrowski, P.C. Ford, Dalton Trans. (2009) 10660–10669.
[4] U. Schatzschneider, Eur. J. Inorg. Chem. (2010) 1451–1467.
[5] R. Bonnett, Chemical Aspects of Photodynamic Therapy, Gordon & Breach, London, U.K, 2000.
[6] M. Ethirajan, Y. Chen, P. Joshi, R.K. Pandey, Chem. Soc. Rev. 40 (2011) 340–362.
[7] M.R. Detty, S.L. Gibson, S.J. Wagner, J. Med. Chem. 47 (2004) 3897–3915.
[8] A.P. Castano, P. Mroz, M.R. Hamblin, Nat. Rev. Cancer 6 (2006) 535–545.
[9] M.C. DeRosa, R.J. Crutchley, Coord. Chem. Rev. 233–234 (2002) 351–371.
[10] I.J. MacDonald, T.J. Dougherty, J. Porphyrins Phthalocyanines 5 (2001) 105–129.
[11] K. Szacilowski, W. Macyk, A. Drzewiecka-Matuszek, M. Brindell, G. Stochel, Chem. Rev. 105 (2005) 2647–2694.
[12] S.I. Moriwaki, J. Misawa, Y. Yoshinari, I. Yamada, M. Takigawa, Y. Tokura, Photodermatol. Photoimmunol. Photomed. 17 (2001) 241–243.
[13] M. Ochsner, J. Photochem, Photobiol. B. Biol. 32 (1996) 3–9.
[14] F.S. Mackay, J.A. Woods, P. Heringová, J. Kašpárková, A.M. Pizarro, S.A. Moggach, S. Parsons, V. Brabec, P.J. Sadler, Proc. Natl. Acad. Sci. U.S.A. 104 (2007) 20743–20748.
[15] A.M. Angeles-Boza, H.T. Chifotides, J.D. Aguirre, A. Chouai, P.K.-L. Fu, K.R. Dunbar, C. Turro, J. Med. Chem. 49 (2006) 6841–6847.
[16] M.J. Rose, N.L. Fry, R. Marlow, L. Hinck, P.K. Mascharak, J. Am. Chem. Soc. 130 (2008) 8834–8846.
[17] (a) S. Swavey, K.J. Brewer, Inorg. Chem. 41 (2002) 6196–6198;
(b) A.A. Holder, S. Swavey, K.J. Brewer, Inorg. Chem. 43 (2004) 303–308.
[18] (a) D.A. Lutterman, P.K.-L. Fu, C. Turro, J. Am. Chem. Soc. 128 (2006) 738–739;
(b) D. Loganathan, H. Morrison, Curr. Opin. Drug Discov. Devel. 8 (2005) 478–486.
[19] N.J. Farrer, J.A. Woods, L. Salassa, Y. Zhao, K.S. Robinson, G. Clarkson, F.S. Mackay, P.J. Sadler, Angew. Chem. Int. Ed. 49 (2010) 8905–8908.
[20] S. Saha, D. Mallick, R. Majumdar, M. Roy, R.R. Dighe, E.D. Jemmis, A.R. Chakravarty, Inorg. Chem. 50 (2011) 2975–2987.
[21] S. Saha, R. Majumdar, M. Roy, R.R. Dighe, A.R. Chakravarty, Inorg. Chem. 48 (2009) 2652–2663.
[22] B. Banik, P.K. Sasmal, S. Roy, R. Majumdar, R.R. Dighe, A.R. Chakravarty, Eur. J. Inorg. Chem. 9 (2011) 1425–1435.
[23] P.K. Sasmal, S. Saha, R. Majumdar, R.R. Dighe, A.R. Chakravarty, Chem. Commun. (2009) 1703–1705.
[24] P.K. Sasmal, A.K. Patra, M. Nethaji, A.R. Chakravarty, Inorg. Chem. 46 (2007) 11112–11121.
[25] J.L. Sessler, R.A. Miller, Biochem. Pharmacol. 59 (2000) 733–939.
[26] W.-H. Wei, Z. Wang, T. Mizuno, C. Cortez, L. Fu, M. Sirisawad, L. Naumovski, D. Magda, J.L. Sessler, Dalton Trans. (2006) 1934–1942.
[27] J.C. Frias, G. Bobba, M.J. Cann, C.J. Hutchison, D. Parker, Org. Biomol. Chem. 1 (2003) 905–907.
[28] E.J. New, D. Parker, D.G. Smith, J.W. Walton, Curr. Opin. Chem. Biol. 14 (2010) 238–246.
[29] E.J. New, D. Parker, Org. Biomol. Chem. 7 (2009) 851–855.
[30] J.C.G. Bunzli, Chem. Rev. 110 (2010) 2729–2755.
[31] A. Datta, K.N. Raymond, Acc. Chem. Res. 42 (2009) 938–947.
[32] P. Caravan, Acc. Chem. Res. 42 (2009) 851–862.
[33] M. Bottrill, L. Kwok, N.J. Long, Chem. Soc. Rev. 35 (2006) 557–571.
[34] A. Hussain, D. Lahiri, M.S.A. Begum, S. Saha, R. Majumdar, R.R. Dighe, A.R. Chakravarty, Inorg. Chem. 49 (2010) 4036–4045.
[35] A. Hussain, S. Saha, R. Majumdar, R.R. Dighe, A.R. Chakravarty, Ind. J. Chem. Sec. A 50A (2011) 519–530.
[36] R.A. Gatenby, R.J. Gillies, Nat. Rev. Cancer 4 (2004) 891–899.
[37] M. Hanif, S.M. Meier, W. Kandioller, A. Bytzek, M. Hejl, C.G. Hartinger, A.A. Nazarov, V.B. Arion, M.A. Jakupec, P.J. Dyson, B.K. Keppler, J. Inorg. Biochem. 105 (2011) 224–231.
[38] S.J. Franklin, Curr. Opin. Chem. Biol. 5 (2001) 201–208.
[39] S.A. Moya, R. Pastene, H.L. Bozec, P.J. Baricelli, A.J. Pardey, J. Gimeno, Inorg. Chim. Acta 312 (2001) 7–14.
[40] W. Leslie, R.A. Poole, P.R. Murray, L.J. Yellowlees, A. Beeby, J.A.G. Williams, Polyhedron 23 (2004) 2769–2777.
[41] B. Arezzini, M. Ferrali, E. Ferrari, C. Frassineti, S. Lazzari, G. Marverti, F. Spagnolo, M. Saladini, Eur. J. Med. Chem. 43 (2008) 2549–2556.
[42] T. Mosmann, J. Immunol. Methods 65 (1983) 55–63.
[43] K. Nakamoto, Infrared and Raman Spectra of Inorganic and Coordination Compounds, third ed. John Wiley & Sons, New York, 1978.
[44] K. Mohri, Y. Watanabe, Y. Yoshida, M. Satoh, K. Isobe, N. Sugimoto, Y. Tsuda, Chem. Pharm. Bull. 51 (2003) 1268–1272.
[45] S. Roy, S. Saha, R. Majumdar, R.R. Dighe, E.D. Jemmis, A.R. Chakravarty, Dalton Trans. 40 (2011) 1233–1242.
[46] (a) D.J. Toffoli, L. Gomes, N.D. Vieira Jr., L.C. Courrol, J. Opt. A: Pure Appl. Opt. 10 (2008) 104026 (8pp);
(b) J.R. Lakowicz, Principles of Fluorescence Spectroscopy, third ed. Springer, New York, 2006.
[47] Y. Fukuda, A. Nakao, K. Hayashi, J. Chem. Soc. Dalton Trans. (2002) 527–533.
[48] H. Krass, E.A. Plummer, J.M. Haider, P.R. Barker, N.W. Alcock, Z. Pikramenou, M.J. Hannon, D.G. Kurth, Angew. Chem. Int. Ed. 40 (2001) 3862–3865.
[49] A.M. Angeles-Boza, P.M. Bradley, P.K.-L. Fu, S.E. Wicke, J. Bacsa, K.R. Dunbar, C. Turro, Inorg. Chem. 43 (2004) 8510–8519.
[50] Y. An, S.-D. Liu, S.-Y. Deng, L.-N. Ji, Z.-W. Mao, J. Inorg. Biochem. 100 (2006) 1586–1593.
[51] J.M. Veal, R.L. Rill, Biochemistry 30 (1991) 1132–1340.
[52] P.A. Pellegrini, J.R. Aldrich-Wright, Dalton Trans. (2003) 176–183.
[53] K.E. Erkkila, D.T. Odom, J.K. Barton, Chem. Rev. 99 (1999) 2777–2795.
[54] A.U. Khan, J. Phys. Chem. 80 (1976) 2219–2227.
[55] M. Tanaka, K. Ohkubo, S. Fukuzumi, J. Phys. Chem. A 110 (2006) 11214–11218.
[56] E. Delaey, F. Van Laar, D. De Vos, A. Kamuhabwa, P. Jacobs, P. De Witte, J. Photochem. Photobiol. B. 55 (2000) 27–36.
[57] (a) J. Portugal, BMC Pharmacol. 9 (2009) 11;
(b) N.J. Wheate, C.R. Brodie, J.G. Collins, S. Kemp, J.R. Aldrich-Wright, Mini Rev. Med. Chem. 7 (2007) 627–648.
[58] (a) T. Storr, K.H. Thompson, C. Orvig, Chem. Soc. Rev. 35 (2006) 534–544;
(b) K.H. Thompson, C. Orvig, Dalton Trans. (2006) 761–764.
[59] R.A. Madina, G.I. Owen, Biol. Res. 35 (2002) 9–26.
[60] M.-W. Louie, H.-W. Liu, M.H.-C. Lam, Y.-W. Lam, K.K.-W. Lo, Chem. Eur. J. 17 (2011) 8304–8308.
[61] D.D. Perrin, W.L.F. Armarego, D.R. Perrin, Purification of Laboratory Chemicals, Pergamon Press, Oxford, 1980.
[62] D.F. Evans, J. Chem. Soc. (1959) 2003–2005.
[63] D.F. Evans, T.A. James, J. Chem. Soc. Dalton Trans. (1979) 723–726.
[64] A.T.R. Williams, S.A. Winfield, J.N. Miller, Analyst 108 (1983) 1067–1071.
[65] N. Walker, D. Stuart, Acta Crystallogr. Sect. A 39 (1983) 158–166.
[66] G.M. Sheldrick, Acta Cryst. A64 (2008) 112–122.
[67] (a) C.K. Johnson, ORTEP-III, Report ORNL–5138, Oak Ridge National Laboratory, Oak Ridge, TN, 1976;
(b) L.J. Farrugia, J. Appl. Cryst. 30 (1997) 565–566.
[68] M.E. Reichmann, S.A. Rice, C.A. Thomas, P. Doty, J. Am. Chem. Soc. 76 (1954) 3047–3053.
[69] J.D. McGhee, P.H. von Hippel, J. Mol. Biol. 86 (1974) 469–489.
[70] M.T. Carter, M. Rodriguez, A.J. Bard, J. Am. Chem. Soc. 111 (1989) 8901–8911.
[71] M.L. Kopka, C. Yoon, D. Goodsell, Proc. Natl. Acad. Sci. U.S.A. 82 (1985) 1376–1380.
[72] S.K. Kim, B. Norden, FEBS Lett. 315 (1993) 61–64.
[73] J. Bernadou, G. Pratviel, F. Bennis, M. Girardet, B. Meunier, Biochemistry 28 (1989) 7268–7275.